PRAMANA — journal of physics
© Indian Academy of Sciences
Vol. 58, Nos 5 & 6
May & June 2002
pp. 743–754

Metals near a magnetic instability

H v LÖHNEYSEN[1,2,*], C PFLEIDERER[1], A SCHRÖDER[3] and O STOCKERT[4]
[1]Physikalisches Institut, Universität Karlsruhe, D-76128 Karlsruhe, Germany
[2]Forschungszentrum Karlsruhe, Institut für Festkörperphysik, D-76021 Karlsruhe, Germany
[3]Department of Physics, Kent State University, Kent, 44242 Ohio, USA
[4]Max-Planck-Institut für chemische Physik fester Stoffe, D-01187 Dresden, Germany
*Email: h.vL@ifp.fzk.de

Abstract. Zero-temperature magnetic phase transitions exhibit an abundance of nearly critical magnetic fluctuations that allow to probe the traditional concepts of the metallic state. For the prototypical heavy-fermion compound, $CeCu_{6-x}Au_x$, a breakdown of the Fermi-liquid properties may be tuned by Au concentration, hydrostatic pressure, or magnetic field. The d-electron weak itinerant ferromagnet $ZrZn_2$, on the other hand, was recently found to display superconductivity in coexistence with ferromagnetism.

Keywords. Heavy fermion systems; ferromagnetism; superconductivity.

PACS Nos 71.10.Hf; 71.27.+a; 74.70.Ad; 75.50.Cc

1. Introduction

Metals with strong electronic correlations close to a magnetic instability have attracted considerable interest in recent years. In a number of these systems, the transition between a paramagnet at high temperature T and a low-T magnetically ordered phase can be tuned to absolute zero by some externally controlled parameters such as chemical composition, pressure, magnetic field, or charge carrier concentration. This offers the possibility to induce a $T = 0$ magnetic–nonmagnetic quantum phase transition (QPT). In the vicinity of this transition, non-Fermi-liquid (NFL) behavior [1] may occur in thermodynamic and transport properties: the linear specific-heat coefficient $\gamma = C/T$ acquires an unusual temperature dependence, often $\gamma \sim -\ln(T/T_0)$, and the T-dependent part of the electrical resistivity $\Delta\rho = \rho - \rho_0$ where ρ_0 is the residual resistivity, often varies as $\Delta\rho \sim T^m$ with $m < 2$, in contrast to the Fermi-liquid predictions $\gamma =$ const. and $m = 2$.

It is generally believed that the NFL behavior observed in heavy-fermion systems (HFS) at the magnetic–nonmagnetic QPT arises from a proliferation of magnetic excitations [2–4]. If the transition is continuous, it is driven by quantum fluctuations instead of thermal fluctuations in finite-T transitions.

$CeCu_{6-x}Au_x$ is one of the best studied examples of NFL behavior at a QPT where macroscopic (thermodynamic and transport properties [5–8]) as well as microscopic measurements (elastic [7] and inelastic neutron scattering [9–11]) have been performed. This system presents very unusual spin dynamics which will be briefly reviewed. We will also discuss how hydrostatic pressure or magnetic field are operative in tuning the system through a QPT.

Very recently, the coexistence of ferromagnetism and superconductivity was demonstrated for UGe_2 for pressures close to the critical pressure where ferromagnetism is suppressed [12]. In addition, the prototype weak itinerant ferromagnet $ZrZn_2$, long considered to be a prime candidate for p-wave superconductivity [13], was finally found to be superconducting in sufficiently pure samples [14]. We will discuss our recent findings on $ZrZn_2$ in the second part of this paper.

2. Non-Fermi liquid behavior and magnetic fluctuations in $\mathbf{CeCu_{6-x}Au_x}$

Pure $CeCu_6$ shows no long-range magnetic order down to very low T due to the quenching of Ce $4f$ magnetic moments by the Kondo effect [15,16]. Several groups have reported evidence for magnetic ordering (either electronic or nuclear) occurring at a few mK [17–19]. With $\gamma = 1.6$ J/mol K^2 it is one of the 'heaviest' HFS. $CeCu_6$ exhibits a pronounced magnetic anisotropy with the magnetization ratios along the three axes $M_c : M_a : M_b \approx 10 : 2 : 1$ at low T [16].

Already at relatively high T, i.e. around 1 K, $CeCu_6$ exhibits intersite antiferromagnetic fluctuations as observed with inelastic neutron scattering (INS) by peaks in the dynamic structure factor $S(\mathbf{q}, \omega)$ for energy transfer $\hbar\omega = 0.3$ meV at $\mathbf{Q} = (1\,0\,0)$ and $(0\,1 \pm 0.15\,0)$ [20,21]. The rather large widths of these peaks correspond to correlation lengths extending roughly only to the nearest Ce neighbors. Recently, additional features in the a^*c^* plane at an energy transfer of 0.1 meV were found [22].

Upon alloying with Au, the $CeCu_6$ lattice expands [23], thus weakening the hybridization between conduction electrons and Ce $4f$ electrons. Hence the conduction electron–$4f$ electron exchange constant J decreases, leading to a stabilization of localized magnetic moments which can now interact via the RKKY interaction, with ensuing antiferromagnetic order [24]. Figure 1 shows the Néel temperature T_N of $CeCu_{6-x}Au_x$ vs. x. The magnetic structure of $CeCu_{6-x}Au_x$ ($0.15 \le x \le 1$) was determined with elastic neutron scattering [7,25,26].

The onset of magnetic order in $CeCu_{6-x}Au_x$ is observed as a kink in C/T, cf. figure 2. For the critical concentration $x_c = 0.1$ the linear specific-heat coefficient depends logarithmically on T, $C/T = a\ \ln(T_0/T)$, between 0.06 and 2.5 K, with $a = 0.58$ J/mol K^2 and $T_0 =$ 6.2 K, the latter corresponding to the Kondo temperature T_K of pure $CeCu_6$ [16]. The magnetic susceptibility $\chi(T)$ of the magnetically ordered samples shows a sharp maximum at T_N, $\chi(T)$ for $x = 0.1$ was found to vary as $\chi \sim 1 - a'\sqrt{T}$ between 0.08 and 3 K [5]. Motivated by INS data (see below), Schröder *et al* showed that the $\chi(T)$ data for $x = 0.1$ can be described very well by a different functional dependence, i.e. $\chi(T)^{-1} - \chi(0)^{-1} = a''T^{\alpha}$ with $\alpha = 0.8$ [9]. This fit extends to 7 K, i.e. to well above T_K.

The abundance of low-energy magnetic excitations when T_N is just tuned to zero, has been suggested early on to cause the NFL behavior at the magnetic instability [5]. However, the $-\ln T$ dependence of C/T and the linear T dependence of ρ (not shown) in $CeCu_{6-x}Au_x$ at the magnetic instability are at variance with spin-fluctuation theories for

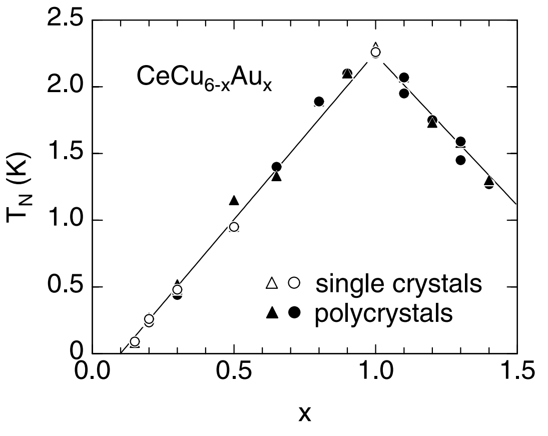

Figure 1. Néel temperature T_N of $CeCu_{6-x}Au_x$ vs. Au concentration x.

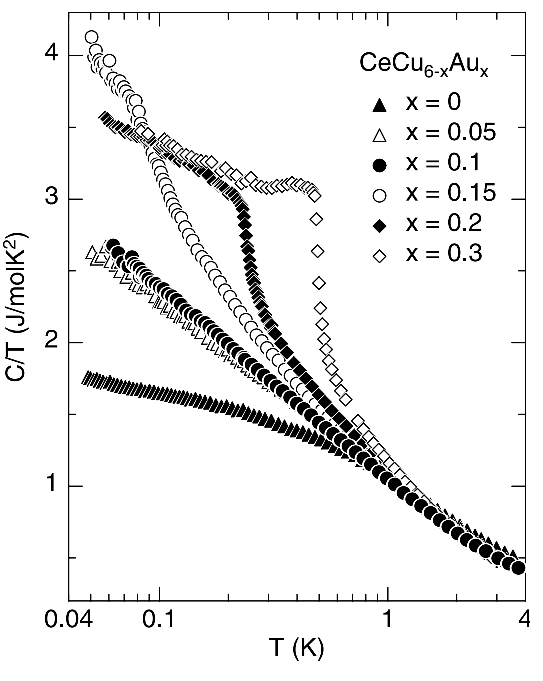

Figure 2. Specific heat C of $CeCu_{6-x}Au_x$ plotted as C/T vs. $\log T$.

three-dimensional (3D) itinerant fermion systems which predict [3,4] $C/T = \gamma_0 - \beta\sqrt{T}$ and $\Delta\rho \sim T^{3/2}$ for antiferromagnets. On the other hand, 2D critical fluctuations coupled to quasiparticles with 3D dynamics do indeed lead to the observed behavior $C/T \sim -\ln\ T$, $\Delta\rho \sim T$, and a linear dependence of T_N or x or p [27].

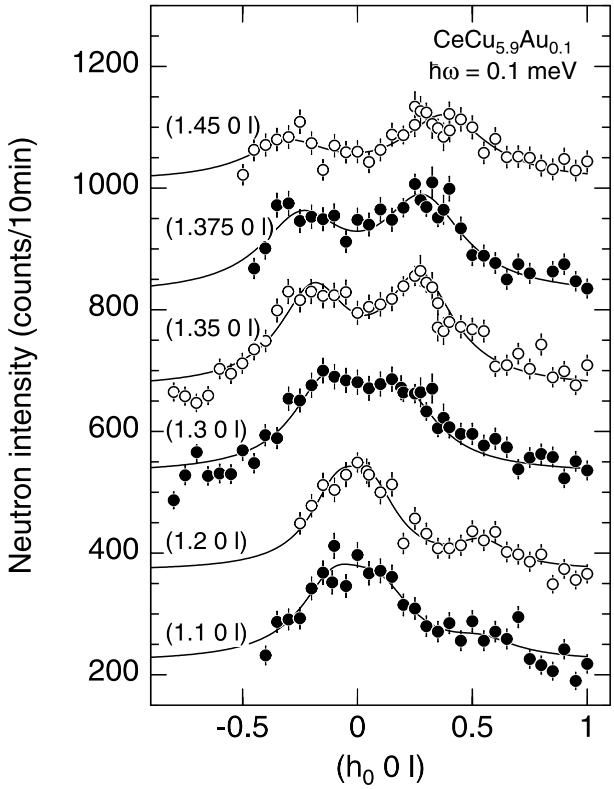

Figure 3. Neutron scattering intensity of $CeCu_{5.9}Au_{0.1}$ (energy transfer $\hbar\omega$=0.1 meV) for different fixed h_0 in the a^*c^* plane at $T = 70$ mK. The scans are shifted by 150 counts/10 min with respect to each other. Solid lines indicate Lorentzian fits with a width 0.24 $Å^{-1}$ for all scans shown.

A detailed INS investigation at the critical concentration $x = 0.1$ [10] showed that the critical fluctuations as measured with an energy transfer of 0.10 meV extend into the a^*c^* plane. This is inferred from a large number of scans, some of which are shown in figure 3. Hence the dynamical structure factor $S(\mathbf{q}, \hbar\omega{=}0.10\text{ meV})$ has the form of rods as indicated by the shaded regions in figure 4.

A quasi-1D dynamic feature in reciprocal space corresponds to quasi-2D fluctuations in real space. The width of $S(\mathbf{q}, \hbar\omega)$ perpendicular to the rods is roughly a factor of five smaller than along the rods [10]. The 3D ordering peaks for $x = 0.15$, 0.2 and 0.3 fall on the rods for $x = 0.1$ which therefore can be viewed as precursors of 3D ordering [7]. From the width of the rods in reciprocal space, the prefactor a of the logarithmic C/T dependence could be calculated to within a factor of two of the experimental value [10].

The spin fluctuations also develop specific dynamics at $x = 0.1$ [9]. The scattering function $S(\mathbf{q}, E, T)$ or the susceptibility $\chi'' = S \cdot (1 - \exp(-E/k_B T))$ exhibit E/T scaling (where $E = \hbar\omega$) in the critical $\mathbf{q}$ region, e.g. at $\mathbf{Q}_c = (0.8, 0, 0)$, which can be expressed

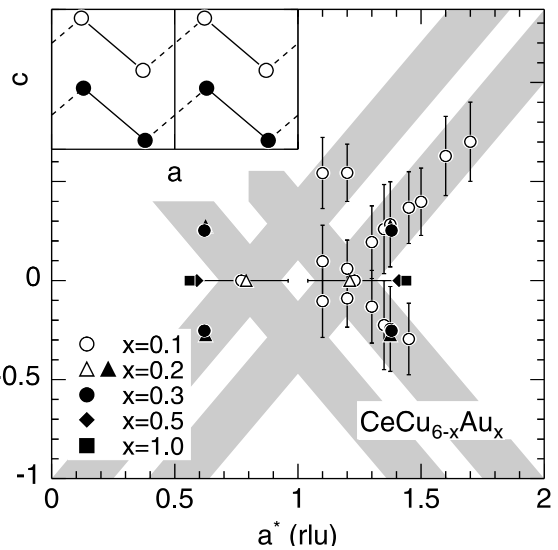

Figure 4. Position of the dynamic correlations ($x = 0.1$, $\hbar\omega = 0.1$ meV, $T < 100$ mK) and magnetic Bragg peaks ($0.2 \leq x \leq 1.0$) in the a^*c^* plane in $CeCu_{6-x}Au_x$. Closed symbols for $x = 0.2$ represent short-range order peaks. The vertical and horizontal bars indicate the Lorentzian linewidths for $x = 0.1$. The four shaded rods are related by the orthorhombic symmetry (we ignore the small monoclinic distortion). The inset shows a schematic projection of the $CeCu_{6-x}Au_x$ structure onto the *ac* plane where only the Ce atoms are shown. The bars in reciprocal space correspond to planes in real space spanned by *b* and the lines in the inset.

by

$$\chi''(\mathbf{Q}_c, E, T) = T^{-\alpha} g(E/k_B T) \tag{1}$$

with $\alpha = 0.75$ [9]. The exponent $\alpha \neq 1$ indicates that the fluctuations do not have a Lorentzian line shape. Figure 5a shows the scaling of $S(\mathbf{q}, E, T)$ for different points in the critical $\mathbf{q}$ region, comprising measurements at Risø (TAS7) and ISIS (IRIS) [11]. Moreover, the anomalous non-Lorentzian response does not change for other $\mathbf{q}$ away from the critical region [11]. For all $\mathbf{q}$ the susceptibility can be expressed as

$$\chi^{-1}(\mathbf{q},\ E,\ T) = c^{-1}(f(\mathbf{q}) + (-\mathrm{i}E + aT)^{\alpha})\,. \tag{2}$$

In particular, the T dependence of the static uniform susceptibility $\chi(\mathbf{q}{=}0, E{=}0)$ yields the exponent $\alpha \approx 0.8$ to a high degree of accuracy, as mentioned above. The simple form of eq. (2) separates static spatial correlations from the specific temporal correlations, the latter being independent of $\mathbf{q}$. These local fluctuations at the quantum critical point show a significant departure from FL behavior since $\alpha < 1$.

Figure 5b shows the collapse of the bulk magnetization data when employing the same scaling function and exponent ($\alpha \approx 0.75$), as those obtained via neutron measurements (see caption of figure 5 for details) [11]. The effective moment $\mu = 1.5\mu_B$ is of the same order as the atomic moment ($0.6\mu_B$) estimated for the $\mathbf{q}$-space average of the neutron data

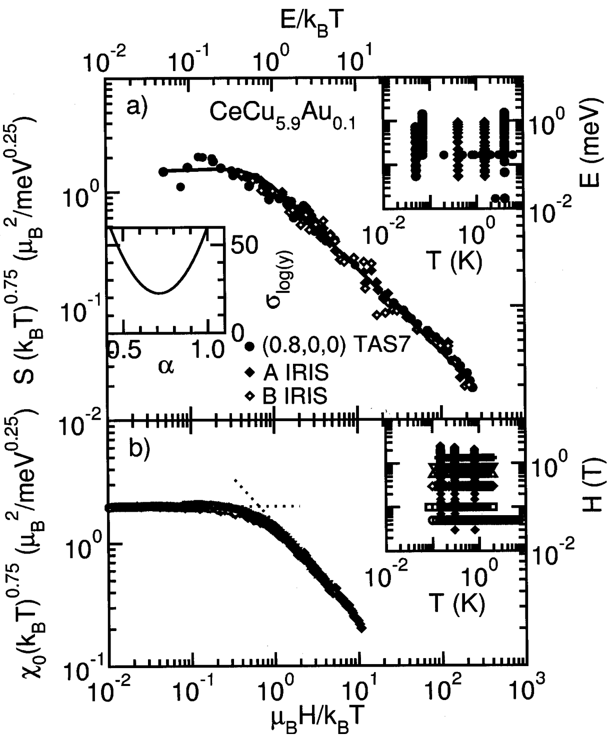

Figure 5. (**a**) E/T scaling plots taken at various critical **q** vectors (labelled as A and B), combining previous triple-axis data with time-of-flight data taken at IRIS. The line is the product of Bose–Einstein factor $[1 - \exp(-E/k_B T)]$ multiplied by the scaling function $g(y) = C/(1 - iy/a)$ with $y = E/T$, scaling factor $a = 0.8\ k_B$ and exponent $\alpha = 0.75$. Right inset shows the wide range of E–T covered. Left inset shows the 'scatter' of the scaling plot as a funtion of α, being minimal for $\alpha = 0.72 \pm 0.05$. (**b**) H/T scaling of the local contribution to the uniform magnetization $M(T, H)$. $1/\chi_0 = (\mathrm{d}M/\mathrm{d}H)^{-1} - (4.1\ \mu_B^2\ \mathrm{meV})^{-1}$. Solid line corresponds to the scaling function $f(h) = (1 + h^2)^{-\alpha/2}$, with $h = \mu_B H/k_B T$ with $\alpha = 0.75$ and an effective moment $\mu = g\mu_B = 1.5\ \mu_B$. Inset shows the H–T range where data were collected and scaling applies.

integrated to $E = 1$ meV. This rules out large, random ferromagnetic clusters as suggested in the Griffiths phase scenario [28]. Thus, the property responsible for the critical behavior is an atomically local magnetic moment, with a size comparable with that of a single spin $S = 1/2$, and with an intrinsically critical response to an external field. The scenario of a locally critical quantum phase transition has received considerable theoretical attention, although a detailed model is not available yet [29,30]. The evolution of the ordered moment with increasing $x > x_c$ [7] may provide a valuable input to test the different models.

The onset of magnetic order in $CeCu_{6-x}Au_x$ is attributed to a weakening of J because of the increase of the molar volume upon alloying with Au as mentioned above. This is confirmed by the observation that T_N of $CeCu_{6-x}Au_x$ decreases roughly linearly under

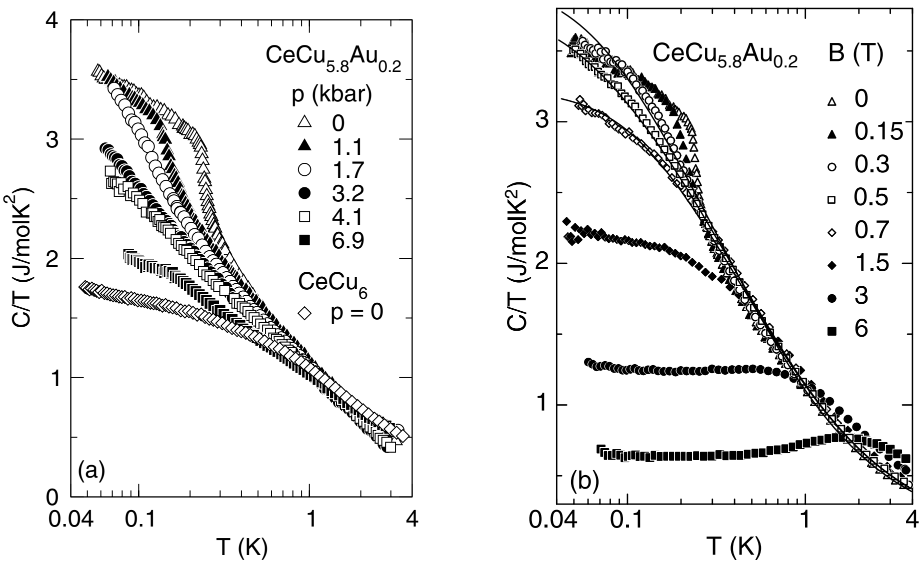

(a) (b)

Figure 6. (**a**) Specific heat C of $CeCu_{5.8}Au_{0.2}$ for different hydrostatic pressures p, plotted as C/T vs. T on a logarithmic scale. Also shown are the data for $CeCu_6$ at ambient pressure. (**b**) C/T vs. T on a logarithmic scale of $CeCu_{5.8}Au_{0.2}$ for different applied magnetic fields B. Solid lines indicate fits of the Moriya–Takimoto model [4] of spin fluctuations to the data for $B = 0.3$, 0.5 and 0.7 T. See text for details.

hydrostatic pressure p [6,31]. Specific heat data for $x = 0.2$, plotted as C/T vs. ln T, are shown in figure 6a for various p. At 3.2–4 kbar C/T exhibits NFL behavior, i.e., $C/T \sim -\ln T$, with the same coefficients a and T_0 as for $x = 0.1$ at $p = 0$. The same holds for $x = 0.3$ at 7–8 kbar [6].

An inducement of NFL behavior in a polycrystalline $CeCu_{4.8}Ag_{1.2}$ alloy by a magnetic field was reported previously, i.e., approximately $C/T \sim -\ln(T/T_0)$ between 0.35 and 2.5 K [32]. For a $CeCu_{5.2}Ag_{0.8}$ single crystal with $T_N = 0.7$ K, at a critical magnetic field $B_c = 2.3$ T applied to the easy direction, C/T varies logarithmically between ~ 1.5 and 0.2 K and then levels off towards lower T, in line with a $\gamma_0 - \beta\sqrt{T}$ dependence [33]. Moreover, the resistivity exhibits a $T^{1.5}$ dependence at B_c. Thus those data appear to be compatible with the conventional spin-fluctuation scenario [4], with $d = 3$ and $z = 2$.

Figure 6b shows the specific heat of $x = 0.2$ for various applied magnetic fields B. Again, T_N is suppressed with increasing B. For fields around $B_c = 0.42$ T determined from elastic neutron scattering [34], we observe a negative curvature in C/T vs. ln T towards low T, distinctly different from the T dependence found in pressure tuning the QPT (cf. figure 6a). Here we have subtracted the hyperfine contribution $C_{hf} = b_N T^{-2}$ due to the Zeeman splitting of ^{63}Cu and ^{65}Cu nuclei. The specific heat data at $B = 0.3$ and 0.5 T may be modeled quite accurately by the self-consistent 3D spin-fluctuation model [4], assuming that this model is appropriate at comparatively small fields. Even the data for $B = 0.7$ T, may be fitted very well. It is remarkable that the agreement reaches as high as 4 K, although the range of validity, in principle, is constrained to temperatures well below the Kondo temperature.

The electrical resistivity $\rho(T)$ for $x = 0.2$ has been investigated for several hydrostatic pressures p (not shown), measured with the electrical current along the a direction, and exhibits a quasi-linear T dependence of $\rho(T)$ for $p = 7$ kbar which resembles that of $\rho(T)$ for $x = 0.1$ at $p = 0$ [35]. On the other hand, application of the magnetic field $B \approx B_c$ yields $\rho(T) = \rho_0 + A''T^m$ with $m = 1.48 \pm 0.03$, in very good agreement with the 3D spin-fluctuation scenario.

The different behavior of $C(T)$ and $\rho(T)$ depending on whether the QPT is tuned by B or p, presents strong evidence for pronounced differences in the fluctuation spectra. The pressure-tuning results suggest that the strongly anisotropic fluctuation spectrum observed for $x = 0.1$ at ambient pressure, which can be modeled by quasi-2D fluctuations, prevails. One may expect that likewise the unexpected energy–temperature scaling of the dynamic susceptibility $\chi^{-1}(q, E) = c^{-1}(f(q) + (-\mathrm{i}E + aT)^{\alpha})$ with $\alpha = 0.75$ observed for $x = 0.1$ at $p = 0$ [9], survives at the QPT under pressure.

On the other hand, magnetic field appears to drive the system towards a more isotropic 3D fluctuation spectrum. However, in view of the strong magnetic anisotropy in $CeCu_{6-x}Au_x$, the transition at B_c might turn out to be of first order. This is also suggested by the B–T phase diagram of $CeCu_{5.8}Au_{0.2}$ [34]. Therefore, it is unclear if the behavior near B_c may indeed be interpreted as a field-induced *quantum* phase transition. INS studies under pressure and in a magnetic field are necessary in order to establish a possible link to the field-temperature scaling of the uniform static susceptibility found for $CeCu_{5.9}Au_{0.1}$ [11] mentioned above.

3. Superconductivity and ferromagnetism in $ZrZn_2$

The compound $ZrZn_2$ is ferromagnetic [36] despite being made from non-magnetic and even superconducting elements. The magnetic properties are believed to derive primarily from the Zr 4d orbitals that have a significant direct overlap [37]. Ferromagnetism develops below the Curie temperature $T_{FM} = 28.5$ K with an ordered moment $\mu_s = 0.17\mu_B$ per formula unit. $ZrZn_2$ has a large electronic heat capacity at low temperatures $C/T \approx 47$ mJ/mol K^2 signaling the presence of many low-energy magnetic excitations in addition to spin waves [38]. The low T_{FM} and small ordered moment make $ZrZn_2$ unique among stoichiometric ferromagnetic metals and indicate that the compound is close to a ferromagnetic QPT. This proximity has led to numerous proposals that $ZrZn_2$ might be a superconductor [13,39].

Figure 7 shows measurements for two $ZrZn_2$ samples of differing quality. The highest-quality sample C has a low-T residual resistivity of $\rho_0 = 0.62$ $\mu\Omega$ cm consistent with a mean free path of a few hundred Ångstroms. Figure 7a shows a rapid drop in the electrical resistivity $\rho(T)$ below T_{SC}=0.29 K suggesting an incomplete transition to a zero-resistance state. The resistance drop is absent in the lower-quality sample A, which has a ρ_0 five times higher than sample C. The application of a field of 0.2 T suppresses the drop as would be expected for a superconducting transition.

A second signature of superconductivity is the Meissner effect. Because $ZrZn_2$ is ferromagnetic, the ac susceptibility $\chi = \mathrm{d}M/\mathrm{d}H$ has a large component due to ferromagnetic domain alignment at low fields. We therefore have subtracted a corresponding T-independent

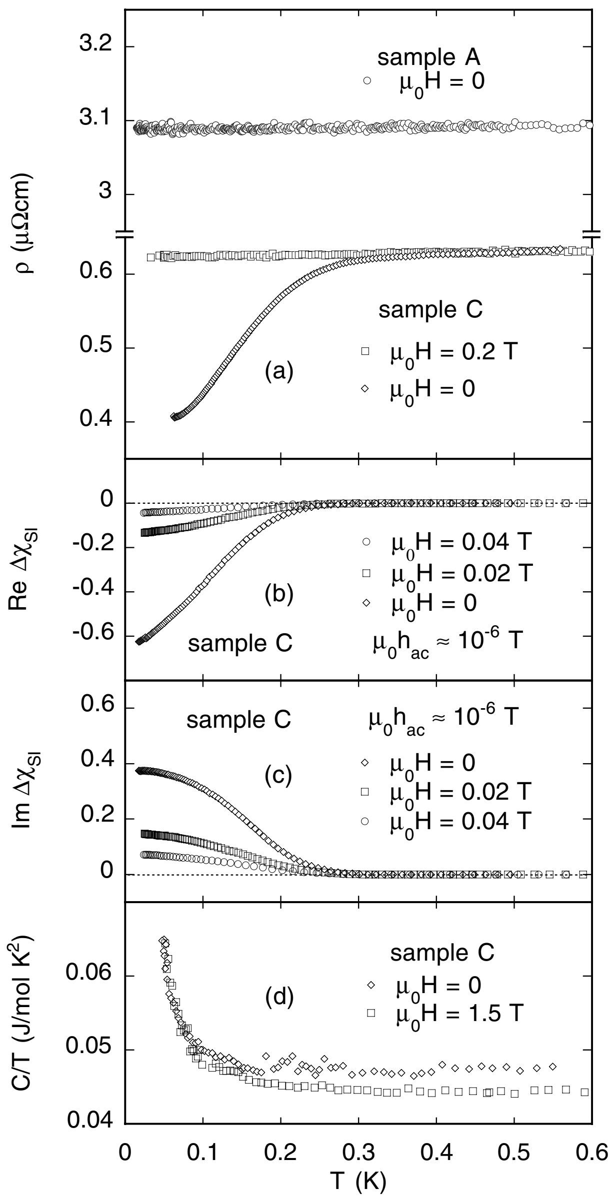

Figure 7. (**a**) Resistivity vs. temperature, $\rho(T)$, at $\mu_0 H = 0$ and 0.2 T of $ZrZn_2$ single crystals. Sample A (non-superconducting) has a five times higher residual resistivity ρ_0. (**b**) Real (reactive) part of the low-amplitude ac susceptibility in SI units vs. temperature for an ac amplitude of 10^{-6} T, Re $\Delta\chi(T)$, at various superposed dc fields after subtraction of the background due to the ferromagnetism. For the lowest excitation amplitudes Re $\Delta\chi(T)$ approaches almost complete diamagnetic shielding: -0.65 (near -1). (**c**) Imaginary (dissipative) part of the ac susceptibility, Im $\Delta\chi(T)$ for sample C. Below T_{SC} a substantial contribution develops, typical of type-II superconductors. (**d**) C/T vs. T of sample C at $\mu_0 H = 0$ and 1.5 T.

(because $T \ll T_{FM}$) background measured above T_{SC}, from our susceptibility data. Figures 7b and c shows the resulting real (reactive) and imaginary (dissipative) parts of the susceptibility, Re $\Delta\chi$ and Im $\Delta\chi$, respectively. A strong diamagnetic signal in Re $\Delta\chi$ associated with superconducting screening is observed below T_{SC}. For the lowest excitation amplitudes, Re $\Delta\chi$ approaches -0.65 as $T \to 0$, comparable with the ideal value of -1. A concomitant increase of the dissipative component Im $\Delta\chi$ is observed, as for other type-II superconductors. The $\chi(T)$ of the low-quality sample A does not exhibit any signs of a diamagnetic contribution. We have also performed SQUID dc magnetization measurements below 1 K on sample C (not shown). The zero-field-cooled dc magnetization corresponds quantitatively to Re $\Delta\chi$, as expected, while the field-cooled magnetization shows a negligible Meissner effect (flux expulsion), as do oxide superconductors.

The low-T specific heat is shown in figure 7d. In the T range around T_{SC} no anomaly is observed, and the normal-state electronic contribution of $C/T = 47$ mJ/mol K^2 prevails. The increase of C/T below 0.15 K is unaffected by the application of a 1.5 T magnetic field, suggesting that it is not associated with superconductivity, but rather with a nuclear contribution.

It has been known for a long time that ferromagnetism in $ZrZn_2$ is rapidly suppressed under pressure p [40]. Figure 8 summarizes the effect of pressure on T_{FM} and T_{SC}. p suppresses both ferromagnetism and superconductivity above a critical pressure of $p_c = 21$ kbar. Thus, it is not sufficient to be close to the ferromagnetic quantum critical point for superconductivity to occur in $ZrZn_2$; the compound must also be in the ferromagnetic state! In view of its sensitivity to the quality of the sample, the superconductivity in $ZrZn_2$ is likely to be unconventional. A further characteristic of the superconducting transition in a ferromagnet may be the absence of a sizable specific heat anomaly hinting at gapless superconductivity. We can exclude scenarios in which the superconductivity is due to inclusions of a second phase or a surface impurity, on the basis of thorough metallurgical tests and because superconductivity and ferromagnetism disappear at the same pressure.

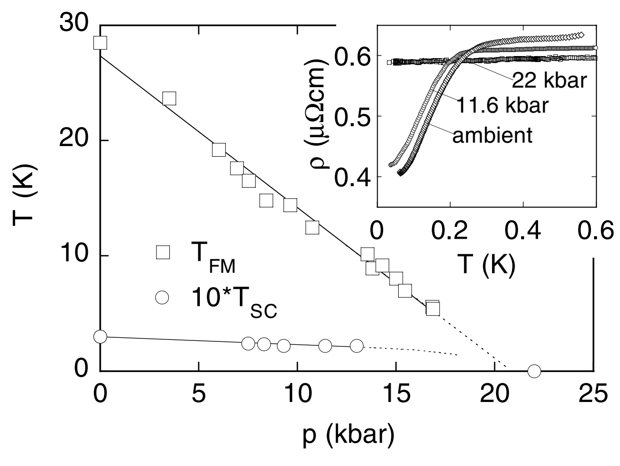

Figure 8. Pressure dependence of the ferromagnetic ordering temperature T_{FM} and T_{SC}. A few typical $\rho(T)$ curves are shown in the inset. Note that T_{SC} for clarity is magnified by a factor of ten.

Our observations in $ZrZn_2$ contrast with materials such as $ErRh_4B_4$ or the recently discovered $RuSr_2GdCu_2O_8$ in which clearly distinguishable subsystems support either ferromagnetism or superconductivity. Furthermore, the presence of superconductivity throughout the entire pressure range for which ferromagnetism exists distinguishes $ZrZn_2$ clearly from UGe_2 [12], which is a strongly uniaxial $5f$ ferromagnet exhibiting coexistence of superconductivity and ferromagnetism over a much smaller pressure range only.

The fact that superconductivity in $ZrZn_2$ only occurs in the presence of ferromagnetism and is hence promoted by the ferromagnetic state, may arise naturally in scenarios where the Cooper pairs are in a parallel-spin (triplet) state, which is already favored in the ferromagnetic state. Such behavior could well be universal for itinerant ferromagnets in the limit of small Curie temperature and long electron mean free path. Further work has to establish the microscopic relation between ferromagnetism and superconductivity.

Acknowledgements

We thank our coworkers and colleagues F Huster, A Neubert, T Pietrus, M Sieck, U Tutsch, M Waffenschmidt and B Will; G Aeppli, N R Bernhoeft, P Coleman, J Flouquet, S M Hayden, A D Huxley, M Loewenhaupt, G G Lonzarich, M B Maple, G Müller-Vogt, N Pyka, A Rosch and P Wölfle for their help and discussions. We would also like to acknowledge the support of the European Science Foundation within the program on Fermi-liquid instabilities in correlated metals (FERLIN) and the Deutsche Forschungsgemeinschaft (DFG).

References

[1] See, e.g.: *Proceedings of the Conference on Non-Fermi-liquid Behavior on Metals*, Santa Barbara 1996, published as special issue of *J. Phys. Condens. Matter* **8**, 9689 (1996)
[2] J A Hertz, *Phys. Rev.* **B14**, 1165 (1976)
[3] A J Millis, *Phys. Rev.* **B48**, 7293 (1993)
[4] T Moriya and T Takimoto, *J. Phys. Soc. Jpn.* **64**, 960 (1995) and refs. therein
[5] H v Löhneysen *et al*, *Phys. Rev. Lett.* **72**, (1994)
[6] B Bogenberger and H v Löhneysen, *Phys. Rev. Lett.* **74**, 1016 (1995)
[7] H v Löhneysen *et al*, *Eur. Phys. J.* **B5**, 447 (1998) and refs. therein
[8] H v Löhneysen, *J. Magn. Magn. Mater.* **200**, 532 (1999)
[9] A Schröder *et al*, *Phys. Rev. Lett.* **80**, 5623 (1998)
[10] O Stockert *et al*, *Phys. Rev. Lett.* **80**, 5627 (1998)
[11] A Schröder *et al*, *Nature* **407**, 351 (2000)
[12] S Saxena *et al*, *Nature* **406**, 587 (2000)
[13] D Fay and J Appel, *Phys. Rev.* **B22**, 3173 (1980)
[14] C Pfleiderer *et al*, *Nature* **412**, 58 (2001); *ibid* **412**, 660 (2001)
[15] Y Onuki and T Komatsubara, *J. Magn. Magn. Mater.* **63&64**, 281 (1987)
[16] A Amato *et al*, *J. Low Temp. Phys.* **68**, 371 (1987)
[17] E A Schuberth *et al*, *Phys. Rev.* **B51**, 12892 (1995)
[18] L Pollack *et al*, *Phys. Rev.* **B52**, R15707 (1995)
[19] H Tsujii *et al*, *Phys. Rev. Lett.* **84**, 5407 (2000)
[20] G Aeppli *et al*, *Phys. Rev. Lett.* **57**, 122 (1986)
[21] J Rossat-Mignod *et al*, *J. Magn. Magn. Mater.* **76&77**, 376 (1988)
[22] O Stockert *et al*, to be published.

[23] T Pietrus *et al*, *Physica* **B206&207**, 317 (1995)
[24] A Germann *et al*, *J. Physique Coll.* **49**, c8-755 (1988)
[25] A Schröder *et al*, *Physica* **B199&200**, 47 (1994)
[26] H Okumura *et al*, *J. Magn. Magn. Mater.* **177–181**, 405 (1998)
[27] A Rosch *et al*, *Phys. Rev. Lett.* **79**, 150 (1997)
[28] A H Castro Neto *et al*, *Phys. Rev. Lett.* **81**, 3531 (1996)
[29] Q Si *et al*, cond-mat/0011477 (2000)
[30] P Coleman *et al*, cond-mat/0105006v3 (2001)
[31] A Germann and H v Löhneysen, *Europhys. Lett.* **9**, 367 (1989)
[32] K Heuser *et al*, *Phys. Rev.* **B57**, R4198 (1998)
[33] K Heuser *et al*, *Phys. Rev.* **B58**, R15959 (1998)
[34] O Stockert *et al*, *Physica B* (in print)
[35] H v Löhneysen *et al*, *Phys. Rev.* **B67**, 134411 (2001)
[36] T B Matthias and R M Bozorth, *Phys. Rev.* **109**, 604 (1958)
[37] T Jarlborg *et al*, *J. Magn. Magn. Mater.* **23**, 291 (1981)
[38] N R Bernhoeft *et al*, *Phys. Scr.* **38**, 191 (1988)
[39] K B Blagoev *et al*, *Phys. Rev. Lett.* **82**, 133 (1998)
[40] T F Smith *et al*, *Phys. Rev. Lett.* **27**, 1732 (1971)